Proceedings World Geothermal Congress 2020+1
Reykjavik, Iceland, April - October 2021

# Budget of Slab-derived Water in Arc Crust: Implications from Crust-Melt Reaction Zones and Fossil Caldera Differentiation Processes

Masaoki Uno, Fajar F. Amanda and Noriyoshi Tsuchiya

Graduate School of Environmental Studies, Tohoku University, Aza-aoba 6-6-20, Aramaki, Aoba, Sendai 980-8579 JAPAN

uno@geo.kankyo.tohoku.ac.jp

**Keywords:** water budget; arc crust; fossil caldera; reaction zone; melt inclusion; supercritical geothermal reservoir.

## ABSTRACT

Water budget in the arc crust is of critical importance for volcanic activities, rheology and geothermal energy budget of the arc crust. Especially, fluid supply by the arc magma is important source of energy for supercritical geothermal reservoirs. According to the geochemical mass balance model, for 1 m along arc distance, 13 t/yr/m $H_2O$ are supplied to sub arc in the form of hydrous melt (Kimura and Nakajima, 2014). However, water budget and its distributions within arc crust have not been well constrained yet. In this study, to understand the re-distribution of $H_2O$ within the arc crust, differentiation of $H_2O$ during crust-melt reactions and subsequent ascent in magma chamber were constrained from crust-melt reaction zones in East Antarctica and melt inclusions in fossil calderas in NE Japan.

The granulite-hosted crust-melt reaction zones in Sør Rondane Mountains, East Antarctica, records granulite–granitic magma reactions under 0.5 GPa, 700°C (Uno et al., 2017). Based on the mineralogical and geochemical analyses of the reaction zones, it is revealed that the fluid infiltrated only ~10 cm from the dike wall towards the crust. The flux of water from the dike to the crust is limited to ~4.2 kg/m$^2$ dike surface. Therefore, it is suggested that most of the $H_2O$ liberated from the granitic dike (more than 65%) was transported as excess fluid toward the upper crust through the dike-related fractures.

The subsequent budget of $H_2O$ transported to upper crust are estimated from fossil calderas distributed in NE Japan arc. Series of Miocene Shirasawa and Fukano calderas (10–6 Ma) consist one of the major fossil caldera clusters in NE Japan. The analyses of melt inclusions in quartz in the calderas suggest that their magma chambers existed at the depth of 1–12 km with dacite–rhyolite melt composition, the $H_2O$ content of melt ranges 3–7 wt% and the magma chamber was water saturated at 1–8 km depth (Suzuki et al., 2017; Amanda et al., 2019). Based on these constraints, the flux of $H_2O$ supplied into the caldera cluster is estimated as 0.4–2.2 × 10$^5$ kg/yr, or 2–11 t/yr/m for a unit along arc distance. This is almost the same order as the subarc $H_2O$ flux estimated by Kimura and Nakajima (2014).

Based on these analyses, 0$^{th}$-order $H_2O$ budget in the arc crust is as follows: most of $H_2O$ liberated from subarc magma (4 wt% $H_2O$; ~13 t/yr/m) do not react with surrounding crust, and transport upwards to magma chambers in upper crust, and get saturated ~8 km (5–6 wt% $H_2O$ melt; 2–11 t/yr/m). Further detailed understanding of mass balance of $H_2O$ is needed with better knowledge of evolution of $H_2O$ content with magma differentiation, and crustal lithology, water content, fracture density and permeability.

## 1. INTRODUCTION

Subduction zones are characterized by the supply of fluids from the subducting slab to the subarc mantle, generation of hydrous melt at subarc, which subsequently ascend to the arc crust. Such hydrous melt is the main forms of $H_2O$ supply to the arc (e.g., Kimura and Nakajima, 2014). The $H_2O$ released from the hydrous magma that emplaced in the upper crust is considered as the source of supercritical geothermal reserviors (Bando et al., 2003; Scott et al., 2015; Tsuchiya et al., 2016; Amanda et al., 2019). The amount and flux of the fluids supplied from the deep crust to the upper-most crust is important for the formation, energy potential and sustainability of supercritical geothermal reservoirs (e.g., Scott et al., 2015).

The main source of $H_2O$ to arc crust is the $H_2O$ liberated through the dehydration of subducting slab. Based on the thermodynamic model of subducting metamorphic rocks, the flux from the dehydrating slab at subarc depth is estimated as 13–57 t/yr/m (for 1 m along arc distance) for NE Japan arc (van Keken et al., 2011; Kimura and Nakajima, 2014). The $H_2O$ liberated from the subducting slab are further transported to lower crust in the form of hydrous melt (~13 t/yr/m; Kimura and Nakajima, 2014).

Based on the petrological and seismological observations, such hydrous melt is generally considered to accumulate at the base of lower crust, and further transported through feeder dikes to lower/upper crust boundary (e.g., Stern, 2002; Takahashi et al., 2013). More evolved, felsic hydrous magma at the lower/upper crust boundary further accumulate to form upper crustal magma chambers (e.g., Stern, 2002). However, up to now, there has not been a comprehensive model on the $H_2O$ budget of the entire arc crust, that describes the amount of generation, supply and consumption of $H_2O$ within arc crust.

To constrain the $H_2O$ budget within arc crust, this study focused on (1) the crust–melt/fluid reaction zones in lower crustal conditions and (2) $H_2O$ supply in the upper crustal magma chambers. Based on the mineralogical and geochemical analyses of the crust–melt/fluid reaction zones, Sør Rondane Mountains, East Antarctica (Uno et al., 2017), we have constrained the $H_2O$ flux during the lower crustal magma ascent. The petrological analyses of fossil magma chambers at NE Japan (Suzuki et al., 2017; Amanda et al., 2019), enable us to quantify the Myr-scale $H_2O$ input to the upper crustal magma chambers. These results are combined to construct 0$^{th}$-order model of the $H_2O$ budget within the arc crust.

## 2. GENERAL MODEL OF ARC CRUST

### 2.1 Geological and Seismic Model of Arc Crust

Arc crust is generally divided into lower and upper crust by the discontinuity of seismic velocity (i.e., conrad discontinuity), where the upper crust is generally considered as andesitic composition and the lower crust as mafic compositions (e.g., Rudnick and Gao, 2003). Geological and petrological observations of crustal sections and volcanic rocks, as well as numbers of seismic observation suggest that basaltic magma generated as subarc accumulates at the base of lower crust. Magma is transported by feeder dikes in the lower crust. More evolved, felsic magma accumulate at the boundary of upper and lower crust, and subsequently ascend to form magma chambers in the upper crust (e.g., Stern, 2002; Takahashi et al., 2013 Figure 1). During the cooling of the upper crustal magma chamber, supercritical saline fluids accumulate at the top of magma chamber (2–5 km in depth), forming a loci of fluid ascent, resulting extensive fluid-rock interaction and formation of porphyri-cupper deposits (e.g., Fournier, 1999; Sillitoe, 2010), which may form the source of supercritical geothermal resources (Tsuchiya et al., 2016; Nohara et al., 2019; Bando et al., 2003; Scott et al., 2015).

In case of north-east Japan, the conrad and moho discontinuity locate at ~18 and ~35 km depth, respectively (e.g., Zhao et al., 1992; Matsubara et al., 2017). In NE Japan, spots of low Vs anomaly occur along the arc at sub arc depth (40–50 km), with ~50 km width and ~100 km spacing, making "hot finger" anomalies, which corresponds to the surface clusters of active volcanos (Tamura et al., 2002). Such hot figures are also characterized by the high seismic attenuation ($Q^{-1}$) are considered as the loci of melt or fluid ascent, i.e., "wet fingers" (Nakajima et al., 2013). Comparisons of seismic tomography with seismic velocity of crustal rocks measured in laboratory under crustal *P-T* conditions suggest that the hot fingers in the lower crust corresponds to the partial melting zones of hornblende grabbro (Nishimoto et al., 2005; Nishimoto et al., 2008; Figure 1 Ishikawa, 2017).

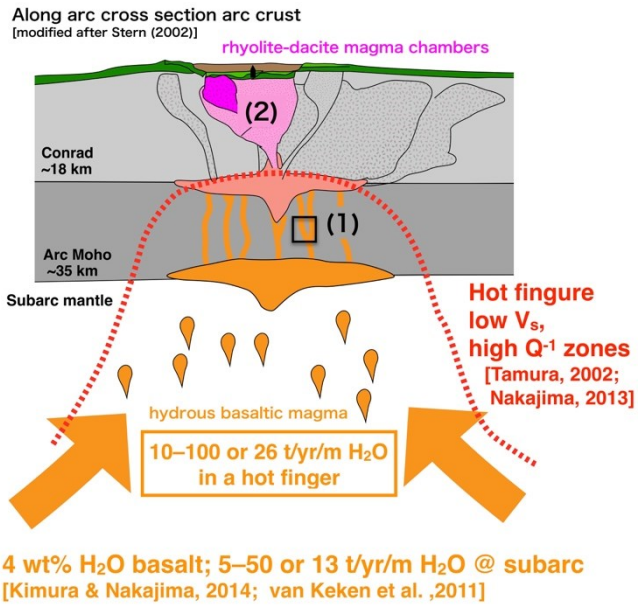


**Figure 1: Schematic, along arc cross section of arc crust (modified after Stern, 2002). Crust–melt/fluid reaction zones (1) and upper crustal magma chambers (2) indicate the schematic location of the focus of this study.**

### 2.2 Water Supply to Subarc

Several models of $H_2O$ budgets along subducting slab suggest that the water input at trench ranges 23–72 t/yr for a 1 m width of slab (t/yr/m; e.g., van Keken et al., 2011; Kimura and Nakajima, 2014). Out of these input at trench, ~7 t/yr/m are expelled by the compaction of pores in the sediments at shallow levels (<30 km), whereas 13–57 t/yr/m of $H_2O$ are released at subarc depth due to the dehydration of the subducting slab and overlying mantle-wedge serpentinites (van Keken et al., 2011; Kimura and Nakajima, 2014). From these $H_2O$ supplied to subarc mantle, ~10 t/yr/m are transported to deeper mantle by the nominally anhydrous minerals (NAMs), whereas other ~5–50 t/yr/m are transported to arc crust in the forms of hydrous melt (~13 t/yr/m at NE Japan; Kimura and Nakajima, 2014). The $H_2O$ contents of hydrous basaltic melt at subarc is universally similar, and is ~4 wt% (e.g., Plank et al., 2013; Kuritani et al., 2014; Kimura and Nakajima, 2014; Figure 1).

Based on the width (~50 km) and spacing (~100 km) of the hot fingers, the subarc magma may concentrate into the hot fingers by the factor of ~2, resulting in supply of 10–100 t/yr/m $H_2O$ in lower crustal hot fingers (Figure. 1).

## 3. $H_2O$ BUDGET AT CRUST–MELT/FLUID REACTION ZONES

### 3.1 Geological Settings of Crust–melt/fluid Reaction Zones

The consumption of $H_2O$ during the magma ascent at lower-middle crust is constrained from the granulite-hosted crust-melt/fluid reaction zones at Sør Rondane Mountains, East Antarctica (Figure 2a; Uno et al., 2017). The Sør Rondane Mountains of eastern Droning Maud Land in East Antarctica are part of Pan-African collision zone between East and West Gondwana (650–500 Ma; Jacobs et al., 2003). The exposure of large crustal sections in this area provides an excellent record of fluid-rock interactions in the crust during the subduction and subsequent collision of East and West Gondwana (e.g., Higashino et al., 2013; Higashino et al., 2019; Kawakami et al., 2017). The sample is located at Balchenfjella, where granulite-facies metamorphic complex that contains biotite-hornblende, biotite- and charnockitic gneisses, migmatites, and ultramafic lenses and granites (e.g., Ishizuka et al., 1993). The samples

were taken from the Berrheia area (72.16253° S, 27.74728° E), which contains hornblende–biotite gneiss and pargasite– phlogopite peridotite units that indicate that both the upper mantle and the lower crust are exposed at the surface.

In the study area, granitic dike distributes ubiquitously, and cut various lithologies including granulite-facies gneiss, migmatite, and peridotite. Of these lithologies, the granitic dike boundaries with pargasite–phlogopite peridotite exhibit the most prominent reaction zones (Figure 2a and b), that record crust–melt/fluid reaction zones at ~0.5 GPa, 700°C (Uno et al., 2017).

### 3.2 Method

The whole sequence of the decimeter scale reaction zones was sampled during the Japan Antarctic Reasearch Expedition 51 (JARE51). Thinsections of the samples were observed under microscope, analyzed by electron probe micro-analyzer (EPMA) for mineral chemistry, and by scanning *X*-ray analytical microscope (SXAM) for elemental distributions. The mineral distributions and $H_2O$ contents along the reaction zones were quantified based on the *X*-ray maps. The details of the analytical conditions are described in Uno et al. (2014b; 2017).

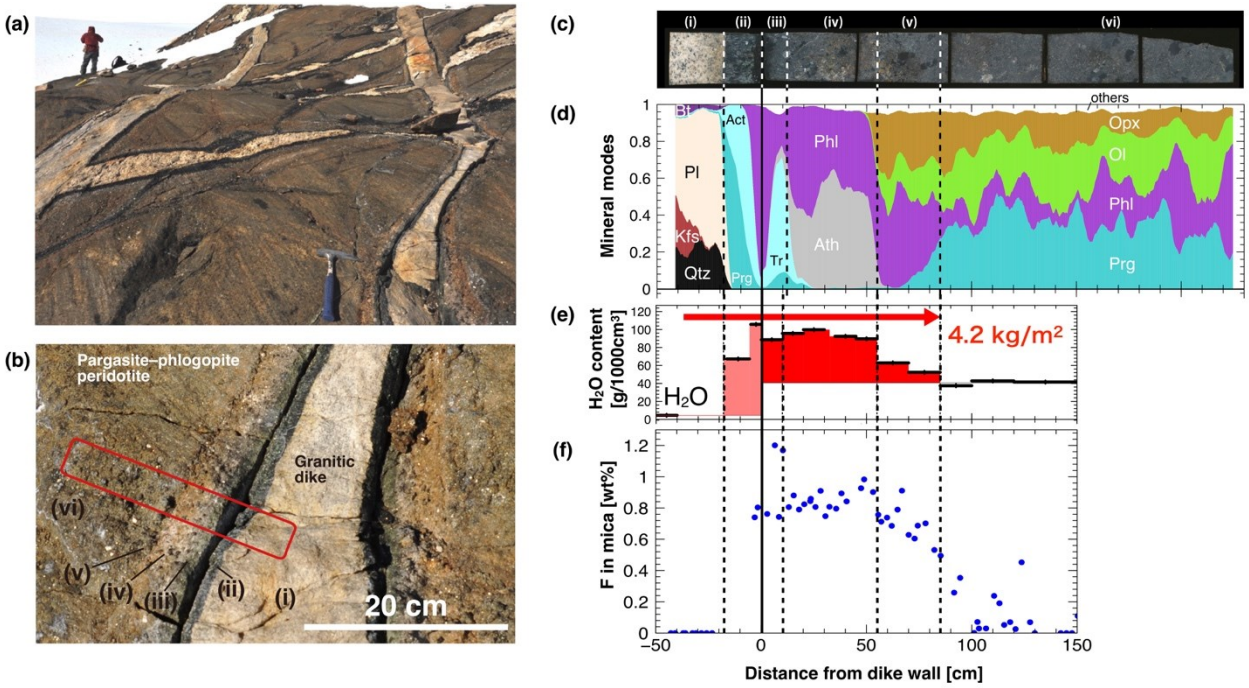


**Figure 2: Crust–melt/fluid reaction zones at Sør Rondane mountains, East Antarctica. (a) Out crop photograph, (b) Close up the reaction zones, (c) Cross section of the rock samples, (d) Mineral modes, (e) $H_2O$ contents, (f) Fluorine contents in phlogopite along the cross section.**

### 3.3 Brief Petrography of Reaction Zones

The dike, reaction zones, and host rock are composed of the following sequence: (i) granitic dike, (ii) pargasite–actinolite zone, (iii) tremolite–phlogopite zone, (iv) anthophyllite–phlogopite zone, (v) phlogopite–olivine–orthopyroxene zone, and (vi) pargasite–phlogopite peridotite host rock (Figure 2b and c). The distribution of minerals, and main mineral assemblage in each zone is shown on Figure 2d. The mineral assemblage and associated $H_2O$ content in the reaction zones changes systematically with distance from the granitic dike toward the host pargasite–phlogopite peridotite. Original crust/melt boundary is suggested at the zone (ii) and (iii) boundary (Uno et al., 2017), based on the distribution of host rock minerals [e.g., absence/existence of Cr-spinel, Cr-rich magnetite and phlogopite porphyroblasts at zone (ii)/zones(iii)–(vi)] and the growth orientations of amphiboles [i.e., perpendicular to dike at zone (ii) and random at zone (iii)–(vi)].

The mineral assemblage of each zone changes sharply at the zone boundaries, except for zone (v) where pargasite mode gradually increase and transits to the host pargasite–phlogopite peridotite. The modes of hydrous minerals (phlogopite, pargasite, anthophyllite, tremolite and actinolite) increases from the host pargasite–phlogopite peridotite towards the pargasite–actinolite zone (Figure 2d).

The $H_2O$ contents increases from the host pargasite–phlogopite peridotite (~40 g/1000 $cm^3$ rock) towards anthophyllite–phlogopite zone (~90 g/1000 $cm^3$ rock), are almost constant till tremolite–actinolite zone, and take slightly lower values at pargasite–actinolite zone (~70 g/1000 $cm^3$ rock) (Figure 2e). The granitic dike has lowest $H_2O$ content (~4 g/1000 $cm^3$ rock) among the reaction zone sequence.

The fluorine contents in phlogopite at zone (ii)/(iii) boundary is ~0.8 wt%, and is almost constant till zone (iv)/(v) boundary, and gradually decrease toward the host pargasite–phlogopite peridotite (0–0.4 wt%) (Figure 2f).

The pargasite–plagioclase and actinolite–plagioclase pairs give *P–T* conditions of ~0.5 GPa and 700°C at the granitic dike/pargasite–actinolite zone boundary. The sets of conventional geothermometry in the host pargasite–phlogopite peridotite also gives ~700°C, representing that the reaction zones occurred at middle–lower crustal *P–T* conditions (Uno et al., 2017)

### 3.4 $H_2O$ Budget during Crust–melt/fluid Reaction Zones

The petrography summarized above suggest that $H_2O$ is supplied to the host pargasite–phlogopite peridotite at the distance of ~10 cm from the original crust/melt boundary (Figure 2). Based on the increase of $H_2O$ content in the zone (iii)–(v) compared to the host pargasite–phlogopite peridotite, the $H_2O$ supply from the granitic melt to the crust is quantified as 4.2 kg per 1 $m^2$ of dike wall (Figure 2e).

### 3.5 $H_2O$ Budget during Magma Ascent in the Lower Crust

Based on the observation above, $H_2O$ consumption during the ascent of granitic magma in the lower crust can be modelled as follows:

$$\chi_{\mathrm{hydration}} = \frac{\mathrm{H_2O\ consumed\ by\ the\ hydration\ of\ crust\ [kg]}}{\mathrm{H_2O\ in\ origial\ magma\ \ [kg]}} = \frac{J_{\mathrm{H2O}}^{\mathrm{hydration}}\, A_{\mathrm{dike}}}{C_{\mathrm{H2O}}^{\mathrm{magma}}\, V_{\mathrm{magma}}} = \frac{2\, J_{\mathrm{H2O}}^{\mathrm{hydration}}}{C_{\mathrm{H2O}}^{\mathrm{magma}}\, R_{\mathrm{magma/dike}}\, W_{\mathrm{dike}}} \quad (1)$$

where $X_{\mathrm{hydration}}$ represent the ratio of mass of $H_2O$ consumed by the hydration over the mass of $H_2O$ contained in the original magma. $J_{\mathrm{H2O}}^{\mathrm{hydration}}$, $C_{\mathrm{H2O}}^{\mathrm{magma}}$ are total flux of $H_2O$ during hydration of crust per unit surface of dike wall [$kg/m^2$], $H_2O$ content in original magma [$kg/m^3$], respectively. $A_{\mathrm{dike}}$, $W_{\mathrm{dike}}$ and $V_{\mathrm{magma}}$ are surface area [$m^2$] and width [m] of dike, and total volume of magma flowed through the dikes [$m^3$]. $R_{\mathrm{magma/dike}}$ represents the volume ratio of total amount of magma over the volume of dike, or "magma/dike volume ratio" (Figure 3a).

$J_{\mathrm{H2O}}^{\mathrm{hydration}}$ is constrained as ~4.2 $kg/m^2$ by the above analysis. The $H_2O$ contents of magma in arc basalt is ~4 wt% (e.g., Plank et al., 2013), and that of granitic melt in the above crust–melt reaction zone is thermodynamically constrained as ~5.0–5.6 wt% (Uno et al., 2017). Considering the density of hydrous rhyolite melt (~2300 $kg/m^3$; e.g., Okumura and Nakashima, 2005), $C_{\mathrm{H2O}}^{\mathrm{magma}}$ is constrained as ~100 $kg/m^3$.

Based on the above constants, $X_{\mathrm{hydration}}$, the ratio of $H_2O$ consumption by hydration over $H_2O$ transport by magma, can be expressed as a function of dike width ($W_{\mathrm{dike}}$) and magma/dike volume ratio ($R_{\mathrm{magma/dike}}$) (Figure 3). Considering the ranges of typical dike width at crustal rocks 0.1–100 m, and geometrical constraints of $R_{\mathrm{magma/dike}} > 1$, the range of $X_{\mathrm{hydration}}$ is constrained as <35%, is and $\ll 10\%$ for most cases (Figure 3). This suggest that $H_2O$ consumption during magma ascent at lower crustal condition is minor, and most of the $H_2O$ contained in the hydrous melt is effectively transported towards the upper crust. This is also supported by the very limited fluid infiltration (~10 cm) and hydration observed for the crust–melt/fluid reaction zones (Figure 2).

Note that this estimation is 0-th order approximation. If hydrofracturing are triggered by the fluids released from the solidifying dike, the reactive surface area of dike increases, which corresponds to the smaller dike width ($W_{\mathrm{dike}}$), resulting in larger $X_{\mathrm{hydration}}$, or larger $H_2O$ consumption by the crust. In contrast, in case the dominant magma transport occurs in the forms of plume rather than dike, the reactive surface area of magma decreases, which corresponds to the larger dike width ($W_{\mathrm{dike}}$), resulting in smaller $X_{\mathrm{hydration}}$, or smaller $H_2O$ consumption by the crust (Figure 3).

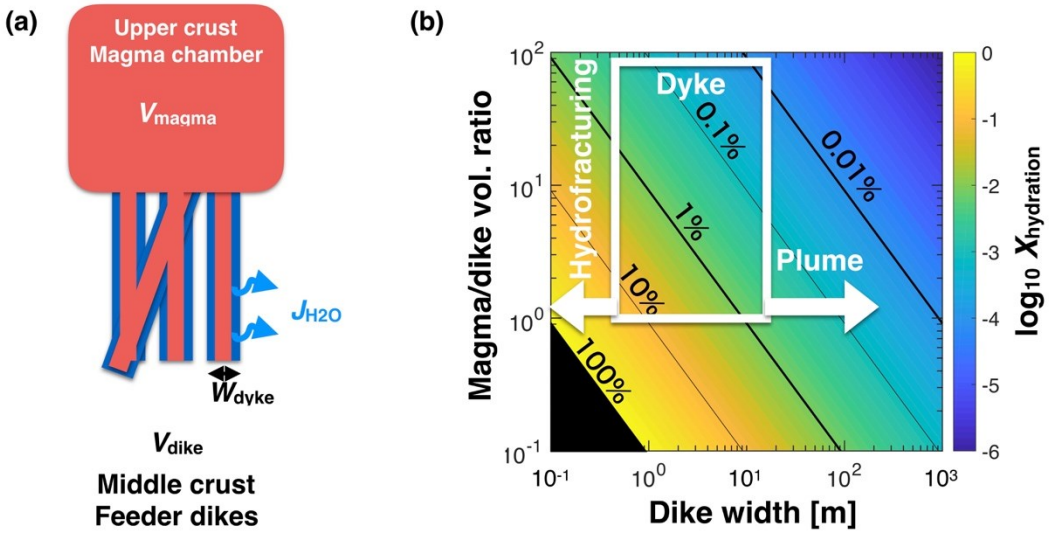


**Figure 3: Model estimates of hydration during the magma ascent from lower crust to upper crustal magma chamber. (a) Schematic model setup, (b) ratio of amount of hydrated $H_2O$ over the original $H_2O$ content of the magma ($X_{\mathrm{hydration}}$), plotted as a function of dike width and magma/dike volume ratio.**

## 4. $H_2O$ SUPPLY AT UPPER-CRUSTAL MAGMA CHAMBERS

### 4.1 Geological Settings of the Studied Fossil Calderas

The amount of $H_2O$ supplied to upper crust is constrained from the mass balance of fossil magma chambers distributed in NE Japan arc. In NE Japan arc, more than 80 late Cenozoic fossil calderas distribute over the arc (Yoshida et al., 2014b). The Miocene Shirasawa and Fukano Calderas are in one of those fossil caldera clusters, located ~20 km east from the present volcanic front. The caldera cluster consists of 10–8 Ma Shirasawa (~20×15 km in diameter) and ~7 Ma Jogi and Fukano (~10×5 km in diameter), and ~1.8 Ma Nanatsumori calderas (~5 km in diameter). These calderas are filled with rhyolitic to dacitic pyroclastic flow deposit. The exposures of these caldera offer an excellent evaluation of the million-year scale evaluation of $H_2O$ budget, which is difficult to constrain from active volcanos where older exposures are difficult to access.

### 4.2 Method

To understand the spatio-temporal variations of chemical compositions of melt in the fossil calderas, total ~40 samples were collected from Shirasawa and Fukano Calderas. The quartz grains were mounted in epoxy, polished for exposures of melt inclusions. Total 619 melt inclusions were analyzed by secondary electron microscopy–energy-dispersive spectroscopy (SEM–EDS) for chemical compositions, and 13 melt inclusions were analyzed by fourier transform–infrared (FT–IR) spectroscopy for $H_2O$ and $CO_2$ contents.

As plagioclase crystallizes earlier than quartz for most volcanic rocks, the melt inclusions in quartz are considered to have equilibrated with both plagioclase and quartz. The crystallization pressures of the host quartz were estimated from the chemical compositions of melt inclusions. This barometry is based on the pressure dependence of the cotectic curve separating the quartz and feldspar stability fields in the rhyolite system Qtz–Ab–Or(–An–$H_2O$) (Blundy and Cashman, 2001). We used the calibration of Wilke et al. (2017) for the pressure dependency on anorthite and $H_2O$ contents. The details of analytical conditions, calculation procedures, and the results of the chemical analyses of these melt inclusions are reported in Suzuki et al. (2017) and Amanda et al. (2019).

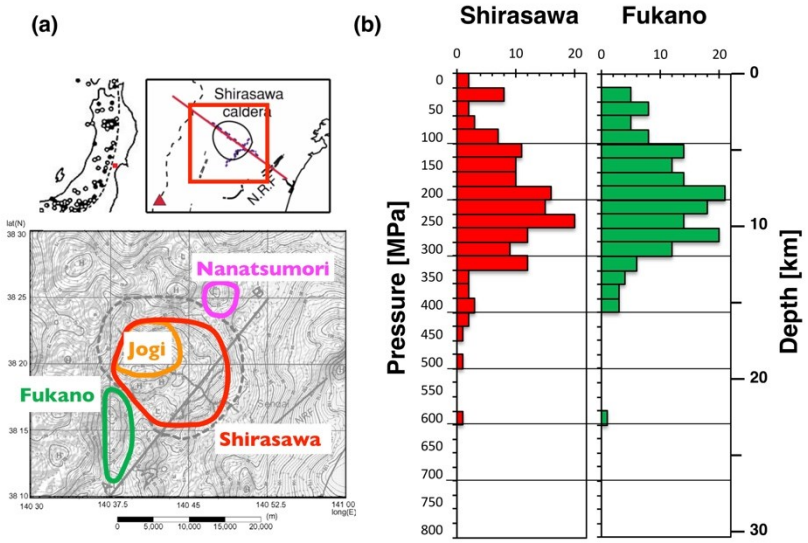


**Figure 4: Fossil caldera cluster at NE Japan and pressures recorded in melt inclusions. (a) Locations of the Shirasawa and Fukano calderas (modified after Komazawa and Mishina, 2002), (b) Frequency of the entrapment pressures of melt inclusions in quartz phenocrysts.**

### 4.3 Depth Structure of Magma Chambers under Fossil Calderas

The $SiO_2$ content of the melt inclusions ranged 60–78 wt%, and are 70–78 wt% for most of the inclusions, and mostly classified as rhyolite or dacite. Most of the melt inclusions are classified as low alkali tholeiite, with some exceptions of high alkali tholeiite. The estimated entrapment pressures of melt inclusion ranges from 2–600 MPa, and they concentrate at around 30–320 MPa for both Shirasawa and Fukano calderas (Figure 4b). Assuming the crustal density of ~2700 kg/m$^3$, these pressures corresponds to 0–12 km depth, suggesting that the magma chamber had existed at this pressure range during the activities of these fossil magma chambers (Figure 4b).

### 4.4 $H_2O$ Contents of the Magma Chambers

The $H_2O$ contents of the melt inclusions ranges 2.8–5.5 wt% (n=4), 6.4 wt% (n=1), and 3.3–7.4 wt% (n=8) for Shirasawa, Jogi and Fukano calderas, respectively. $CO_2$ were detected for only two samples (38 and 19 ppm), and $CO_2$ contents of the other samples were lower than the detection limit (<~15 ppm). The Figure 5 shows the comparisons of pressure determined by the Qtz–Pl–melt equilibria (MI entrapment pressure) and the $H_2O$ contents of melt inclusions. The pressure–$H_2O$ content relations are consistent with the $H_2O$ saturation curve (Liu et al., 2005) assuming ~700°C. These relations suggest that the melt of the Shirasawa and Fukano calderas are saturated with $H_2O$ at pressures <150–200 MPa (<8 km). Maximum $H_2O$ contents of the melt were 5–6 wt% and ~7 wt% for Shirawa and Fukano calderas, respectively.

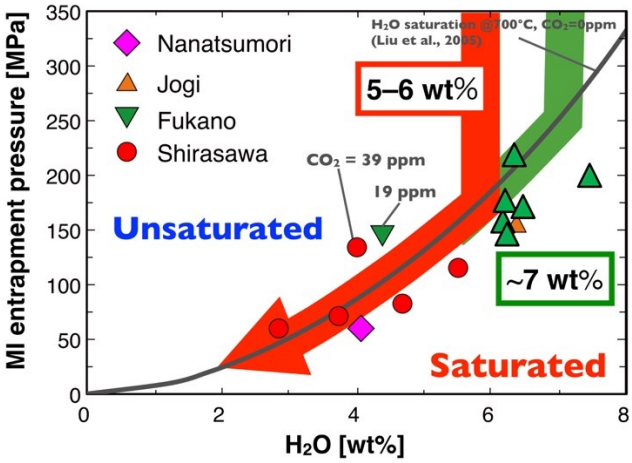


**Figure 5: Relations of $H_2O$ contents and entrapment pressures of melt inclusions estimated from quartz–plagioclase–melt equilibria.**

### 4.5 $H_2O$ Flux into Fossil Calderas and Caldera Clusters

Based on the above parameters constrained for Shirasawa and Fukano caldera, the Myr-scale $H_2O$ flux into these fossil calderas can be estimated. Shirasawa caldera is characterized by the diameter of 15–20 km (gravity anomalies; Komazawa and Mishina, 2002), depth range of magma chamber of 7–10 km (Figure 3b), primary $H_2O$ contents in rhyolite melt of 5–6 wt% (Figure 4b), and caldera duration of 2–3 Myr (K-Ar and zircon U-Pb dating; Fujiwara et al., 2014) (K-Ar and zircon U-Pb dating; Fujiwara et al., 2013). This results in the $H_2O$ flux of 0.5–2.2 × $10^5$ t/yr towards the magma chamber of Shirasawa caldera, corresponding to 3.1–10.8 t/yr/m arc length. Estimates for Fukano caldera is also consistent, with 9.7–10.0×4.7–5.0 km diameter (Figure 4a), ~8 km depth range of magma chamber (Figure 3b), 3–7 wt% of $H_2O$ in the rhyolite melt (Figure 4b), resulting in 2.3–7.6 t/yr/m arc length. Therefore, the independent estimates of $H_2O$ flux at Shirasawa and Fukano caldera matches in the order of 2–11 t/yr/m.

The numbers of fossil of calderas in NE Japan suggest that approximately 10 calderas occur in a hot finger region in ~5 Myrs (e.g., Yoshida et al., 2014a). Assuming average caldera size similar to Shirasawa caldera (~20 km in diameter) and width of a hot finger as ~50 km, the $H_2O$ supply to the hot finger in ~5 Myr can be estimated as 4–17 t/yr/m arc length. This estimate of $H_2O$ flux into upper crust is fewer than, but within ~2 factor differences from the independent estimates of subarc $H_2O$ flux into hot finger of 10–100 t/yr/m $H_2O$ (global estimates; van Keken, 2011) and 26 t/yr/m $H_2O$ for NE Japan (Kimura and Nakajima, 2014).

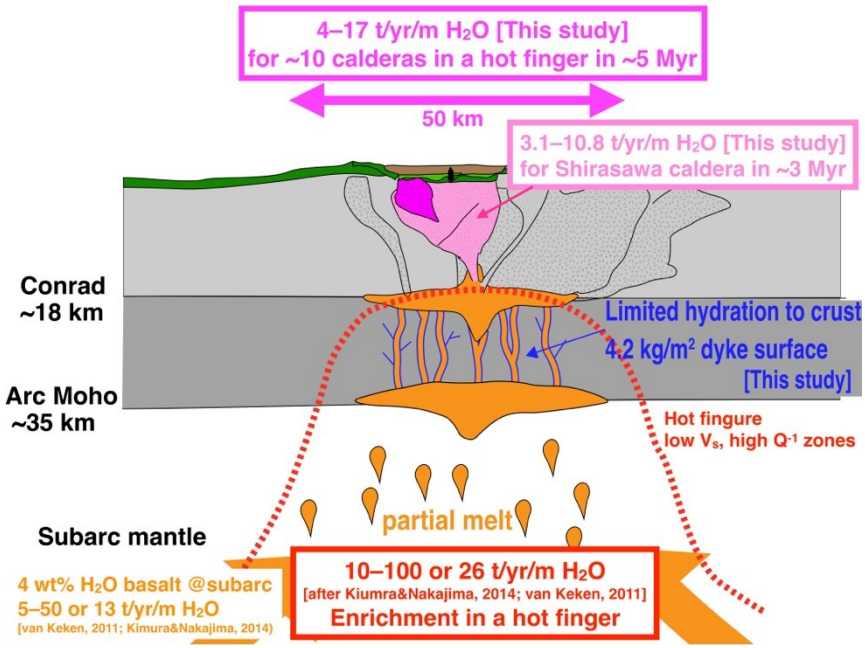


**Figure 6: Summary of the water budget in arc crust constrained by this study and previous studies.**

## 5. 0-TH ORDER MODEL FOR $H_2O$ BUDGET IN THE ARC CRUST

The above-mentioned constraints on the $H_2O$ budget in the arc crust allow us to depict 0-th order model for the $H_2O$ budget in the arc crust:

(1) Supply of $H_2O$ at the base of arc crust are mainly sourced from hydrous basaltic magma generated at subarc, with average $H_2O$ content of ~4wt% (5–50 t/yr/m or ~13 t/yr/m $H_2O$). The hydrous magma accumulates into hot fingers (~50 km width, ~100 km spacing), resulting flux of $H_2O$ of 10–100 t/yr/m or 26 t/yr/m under a hot finger.

(2) The $H_2O$ loss from dike wall during the ascent of magma from lower crust is limited in the scale of ~10 cm, due to the very low intact permeability of the crustal material. $H_2O$ loss, or hydration flux is ~4.2 kg per 1 $m^2$ of dike wall. For ranges of magma/dyke ratio and dike width, total $H_2O$ loss is limited to $\ll$ 10% of the $H_2O$ content of the original magma. This means that most of the $H_2O$ supplied to the base of crust can be effectively transported into upper crust. However, if hydrofracturing occur during the ascent of the magma, reactive surface area of dike increases, and $H_2O$ loss would be higher.

(3) The hydrous magma ascent to the upper crust and get saturated at ~8 km (5–7 wt% $H_2O$ melt). The Myr-scale $H_2O$ supply into single caldera is ~2–11 t/yr/m. For a volcanic cluster, the average $H_2O$ supply would be 4–17 t/yr/m. This estimate is fewer than the estimates of supply of $H_2O$ at the base of a hot finger (1), but matches within ~2 factor differences.

The results of this study show that supply of $H_2O$ at the base of crust and those at the upper crustal magma chamber matches within the factor of ~2, suggesting that subarc $H_2O$ can be effectively transported to the upper crust. The effective transport of $H_2O$ from subarc mantle to the surface are consistent with high $^3He/^4He$ observed for backarc hot springs (Horiguchi et al., 2010). Minor consumption of $H_2O$ within the arc crust is also consistent with billion year-scale stability of ocean and effective return of subducted $H_2O$ to the earth's surface (e.g., Plümper et al., 2016).

The results of this study support the hypothesis that hydrous magma is the main source of transportation of $H_2O$ into the upper crust. As this study focused on the felsic magma chamber in the upper crust, uncertainty remains in the changes of $H_2O$ content from basaltic magma to felsic magma during the ascent from subarc to upper crust, and the absolute amount of felsic magma supplied to upper crust. Non-volcanic, mantle-derived fluid activities are another factor that should be taken into account in the future model, as they are widely recognized in the crust during lower crustal retrogressive metamorphism (e.g., Uno et al., 2014a; Uno et al., 2015; Uno and Kirby, 2019; Yoshida et al., 2015) and as Arima-type hot springs (e.g., Kusuda et al., 2014; Morikawa et al., 2016).

## 6. CONCLUSION

As an attempt to constrain the deep sources of supercritical geothermal reservoir, $0^{th}$-order model of water budget in arc crust was constructed through the mass balance analyses of crust–melt/fluid reaction zones and upper crustal magma chambers. At the base of arc crust, $H_2O$ is supplied in the forms of hydrous basaltic melt with ~4wt% $H_2O$ and a flux of 5–50 or ~13 t/yr/m. These fluxes are expected to concentrate by a factor of ~2 under the hot finger areas (10–100 or ~26 t/yr/m). Mass balance analyses of crust–melt/fluid reaction zones show that the hydration of the crust is limited at a total flux of ~4.2 kg $H_2O/m^2$ dike surface. As a results, >65% (>90% for most cases) of $H_2O$ in the subarc magma is expected to be transported to the upper crust. The Myr-scale $H_2O$ flux from the hydrous magma observed at fossil caldera magma chambers is ~2–11 t/yr/m, and those for a caldera cluster is estimated as 4–17 t/yr/m. The results of this study suggest that subarc flux and upper crustal flux of $H_2O$ are largely consistent by a factor of ~2, and the subarc $H_2O$ are effectively transported to upper crust in the form of hydrous magma. Further understanding on the magma differentiation, and crustal lithology, water content, fracture density and permeability are needed for better estimation, as well as the role of non-volcanic $H_2O$ fluids on the budget of $H_2O$ in arc crust.

## REFERENCES

Amanda, F.F., Yamada, R., Uno, M., Okumura, S., and Tsuchiya, N., 2019, Evaluation of Caldera Hosted Geothermal Potential during Volcanism and Magmatism in Subduction System, NE Japan: Geofluids, v. 2019, no. 3031586, p. 1–14, doi: 10.1155/2019/3031586.

Bando, M., Bignall, G., Sekine, K., and Tsuchiya, N., 2003, Petrography and uplift history of the Quaternary Takidani Granodiorite: could it have hosted a supercritical (HDR) geothermal reservoir? Journal of Volcanology and Geothermal Research, v. 120, no. 3–4, p. 215–234, doi: 10.1016/S0377-0273(02)00399-2.

Blundy, J.D., and Cashman, K., 2001, Ascent-driven crystallisation of dacite magmas at Mount St Helens, 1980–1986: Contributions to Mineralogy and Petrology, v. 140, p. 631–650, doi: 10.1007/s004100000219.

Fournier, R.O., 1999, Hydrothermal processes related to movement of fluid from plastic into brittle rock in the magmatic-epithermal environment: Economic Geology, v. 94, no. 8, p. 1193–1211, doi: 10.2113/gsecongeo.94.8.1193.

Fujiwara, O., Suzuki, N., Hayashi, H., and Irizuki, T., 2014, Middle to Upper Miocene and Pliocene sequences of southwest Sendai, as a standard referential stratigraphy in the Pacific side of NE Japan: The Journal of the Geological Society of Japan, v. 119, no. Supplement, p. S96–S119, doi: 10.5575/geosoc.2013.0032.

Higashino, F., Kawakami, T., Satish-Kumar, M., Ishikawa, M., Maki, K., Tsuchiya, N., Grantham, G.H., and Hirata, T., 2013, Chlorine-rich fluid or melt activity during granulite facies metamorphism in the Late Proterozoic to Cambrian continental collision zone-An example from the Sør Rondane Mountains, East Antarctica: Precambrian Research, v. 234, p. 229–246, doi: 10.1016/j.precamres.2012.10.006.

Higashino, F., Kawakami, T., Tsuchiya, N., Satish-Kumar, M., Ishikawa, M., Grantham, G., Sakata, S., and Hirata, T., 2019, Brine Infiltration in the Middle to Lower Crust in a Collision Zone: Mass Transfer and Microtexture Development Through Wet Grain-Boundary Diffusion: Journal of Petrology, v. 60, no. 2, p. 329–358, doi: 10.1093/petrology/egy116.

Horiguchi, K., Ueki, S., Sano, Y., Takahata, N., Hasegawa, A., and Igarashi, G., 2010, Geographical distribution of helium isotope ratios in northeastern Japan: Island Arc, v. 19, no. 1, p. 60–70, doi: 10.1111/j.1440-1738.2009.00703.x.

Ishikawa, M., 2017, Deep crustal and uppermost mantle lithology of Island Arcs: Izu Arc and NE Honshu Arc: The Journal of the Geological Society of Japan, v. 123, no. 6, p. 355–364, doi: 10.5575/geosoc.2017.0027.

Ishizuka, H., Asami, M., Grew, E.S., Kojima, H., Makimoto, H., Moriwaki, Y., Osanai, Y., Owada, M., Sakiyama, T., Shiraishi, K., Tainosho, Y., Takahashi, Y., Toyoshima, T., and Tsuchiya, N., 1993, Geological map of Bergersenfjella, Sør Rondane Mountains, Antarctica: Antarctica Geological Map Series, v. Sheet 33, p. National Institute of Polar Research., Tokyo.

Jacobs, J., Bauer, W., and Fanning, C.M., 2003, Late Neoproterozoic/Early Palaeozoic events in central Dronning Maud Land and significance for the southern extension of the East African Orogen into East Antarctica: Precambrian Research, v. 126, no. 1–2, p. 27–53, doi: 10.1016/S0301-9268(03)00125-6.

Kawakami, T., Higashino, F., Skrzypek, E., Satish-Kumar, M., Grantham, G., Tsuchiya, N., Ishikawa, M., Sakata, S., and Hirata, T., 2017, Prograde infiltration of Cl-rich fluid into the granulitic continental crust from a collision zone in East Antarctica (Perlebandet, Sør Rondane Mountains): Lithos, v. 274–275, p. 73–92, doi: 10.1016/j.lithos.2016.12.028.

van Keken, P.E., Hacker, B.R., Syracuse, E.M., and Abers, G. a., 2011, Subduction factory: 4. Depth-dependent flux of $H_2O$ from subducting slabs worldwide: Journal of Geophysical Research, v. 116, no. B1, doi: 10.1029/2010JB007922.

Kimura, J.-I., and Nakajima, J., 2014, Behaviour of subducted water and its role in magma genesis in the NE Japan arc: A combined geophysical and geochemical approach: Geochimica et Cosmochimica Acta, v. 143, p. 165–188, doi: 10.1016/j.gca.2014.04.019.

Komazawa, M., and Mishina, M., 2002, Caldera structure inferred from gravity anomalies west of Nagamachi-Rifu fault, northeast Japan: Earth, Planets and Space, v. 54, no. 11, p. 1049–1053.

Kuritani, T., Yoshida, T., Kimura, J.I., Hirahara, Y., and Takahashi, T., 2014, Water content of primitive low-K tholeiitic basalt magma from Iwate Volcano, NE Japan arc: Implications for differentiation mechanism of frontal-arc basalt magmas: Mineralogy and Petrology, v. 108, no. 1, p. 1–11, doi: 10.1007/s00710-013-0278-2.

Kusuda, C., Iwamori, H., Nakamura, H., Kazahaya, K., and Morikawa, N., 2014, Arima hot spring waters as a deep-seated brine from subducting slab: Earth, Planets and Space, v. 66, no. 1, p. 119, doi: 10.1186/1880-5981-66-119.

Matsubara, M., Sato, H., Ishiyama, T., and Van Horne, A., 2017, Configuration of the Moho discontinuity beneath the Japanese Islands derived from three-dimensional seismic tomography: Tectonophysics, v. 710–711, p. 97–107, doi: 10.1016/j.tecto.2016.11.025.

Morikawa, N., Kazahaya, K., Takahashi, M., Inamura, A., Takahashi, H.A., Yasuhara, M., Ohwada, M., Sato, T., Nakama, A., Handa, H., Sumino, H., and Nagao, K., 2016, Widespread distribution of ascending fluids transporting mantle helium in the fore-arc region and their upwelling processes: Noble gas and major element composition of deep groundwater in the Kii Peninsula, southwest Japan: Geochimica et Cosmochimica Acta, v. 182, p. 173–196, doi: 10.1016/j.gca.2016.03.017.

Nakajima, J., Hada, S., Hayami, E., Uchida, N., Hasegawa, A., Yoshioka, S., Matsuzawa, T., and Umino, N., 2013, Seismic attenuation beneath northeastern Japan: Constraints on mantle dynamics and arc magmatism: Journal of Geophysical Research: Solid Earth, v. 118, no. 11, p. 5838–5855, doi: 10.1002/2013JB010388.

Nishimoto, S., Ishikawa, M., Arima, M., and Yoshida, T., 2005, Laboratory measurement of P-wave velocity in crustal and upper mantle xenoliths from Ichino-megata, NE Japan: Ultrabasic hydrous lower crust beneath the NE Honshu arc: Tectonophysics, v. 396, no. 3–4, p. 245–259, doi: 10.1016/j.tecto.2004.12.010.

Nishimoto, S., Ishikawa, M., Arima, M., Yoshida, T., and Nakajima, J., 2008, Simultaneous high P-T measurements of ultrasonic compressional and shear wave velocities in Ichino-megata mafic xenoliths: Their bearings on seismic velocity perturbations in lower crust of northeast Japan arc: Journal of Geophysical Research: Solid Earth, v. 113, no. 12, p. 1–18, doi: 10.1029/2008JB005587.

Nohara, T., Uno, M., and Tsuchiya, N., 2019, Enhancement of Permeability Activated by Supercritical Fluid Flow through Granite: Geofluids, v. 2019, p. accepted.

Plank, T., Kelley, K. a., Zimmer, M.M., Hauri, E.H., and Wallace, P.J., 2013, Why do mafic arc magmas contain ~4wt% water on average? Earth and Planetary Science Letters, v. 364, p. 168–179, doi: 10.1016/j.epsl.2012.11.044.

Plümper, O., John, T., Podladchikov, Y.Y., Vrijmoed, J.C., and Scambelluri, M., 2016, Fluid escape from subduction zones controlled by channel-forming reactive porosity: Nature Geoscience, v. 1, no. December, doi: 10.1038/NGEO2865.

Rudnick, R., and Gao, S., 2003, Composition of the continental crust, *in* Treatise on geochemistry 3: The Crust, Elsevier Ltd., p. 1–64.

Scott, S., Driesner, T., and Weis, P., 2015, Geologic controls on supercritical geothermal resources above magmatic intrusions.: Nature communications, v. 6, p. 7837, doi: 10.1038/ncomms8837.

Sillitoe, R.H., 2010, Porphyry copper systems: Economic Geology, v. 105, no. 1, p. 3–41, doi: 10.2113/gsecongeo.105.1.3.

Stern, R.J., 2002, Subduction zones: Reviews of Geophysics, v. 40, no. 4, p. 1012, doi: 10.1029/2001RG000108.

Suzuki, T., Uno, M., Okumura, S., Yamada, R., and Tsuchiya, N., 2017, Differentiation of eruptive magma in the late Miocene Shirasawa Caldera and present geothermal reservoir: 日本地熱学会誌, v. 39, no. 1, p. 1–14, doi: 10.11367/grsj.39.25.

Takahashi, T., Hirahara, Y., Miyazaki, T., Senda, R., Chang, Q., Kimura, J.I., and Tatsumi, Y., 2013, Primary magmas at thevolcanic front of the NE Japan arc: Coeval eruption of crustal low-K tholeiitic and mantle-derived medium-K calc-alkaline basalts at Azumavolcano: Journal of Petrology, v. 54, no. 1, p. 103–148, doi: 10.1093/petrology/egs065.

Tamura, Y., Tatsumi, Y., Zhao, D., Kido, Y., and Shukuno, H., 2002, Hot fingers in the mantle wedge: new insights into magma genesis in subduction zones: Earth and Planetary Science Letters, v. 197, p. 105–116.

Tsuchiya, N., Yamada, R., and Uno, M., 2016, Supercritical geothermal reservoir revealed by a granite–porphyry system: Geothermics, v. 63, p. 182–194, doi: 10.1016/j.geothermics.2015.12.011.

Uno, M., Iwamori, H., Nakamura, H., Yokoyama, T., Ishikawa, T., and Tanimizu, M., 2014a, Elemental transport upon hydration of basic schists during regional metamorphism: Geochemical evidence from the Sanbagawa metamorphic belt, Japan: Geochemical Journal, v. 48, no. 1, p. 29–49, doi: 10.2343/geochemj.2.0283.

Uno, M., Iwamori, H., and Toriumi, M., 2015, Transition from dehydration to hydration during exhumation of the Sanbagawa metamorphic belt, Japan, revealed by the continuous P–T path recorded in garnet and amphibole zoning: Contributions to Mineralogy and Petrology, v. 170, no. 3, p. 33, doi: 10.1007/s00410-015-1185-9.

Uno, M., and Kirby, S., 2019, Evidence for multiple stages of serpentinization from the mantle through the crust in the Redwood City Serpentinite mélange along the San Andreas Fault in California: Lithos, v. 334–335, p. 276–292, doi: 10.1016/j.lithos.2019.02.005.

Uno, M., Okamoto, A., and Tsuchiya, N., 2017, Excess water generation during reaction-inducing intrusion of granitic melts into ultramafic rocks at crustal P–T conditions in the Sør Rondane Mountains of East Antarctica: Lithos, v. 284–285, p. 625–641, doi: 10.1016/j.lithos.2017.04.016.

Uno, M., Okamoto, A., and Tsuchiya, N., 2014b, Millimeter– to decimeter– scale compositional mapping using a scanning X–ray analytical microscope and its application to a reaction zone in high–grade metamorphic rock: Journal of Mineralogical and Petrological Sciences, v. 109, no. 6, p. 271–278, doi: 10.2465/jmps.140613b.

Wilke, S., Holtz, F., Neave, D.A., and Almeev, R., 2017, The effect of anorthite content and water on quartz-feldspar cotectic compositions in the rhyolitic system and implications for geobarometry: Journal of Petrology, v. 58, no. 4, p. 789–818, doi: 10.1093/petrology/egx034.

Yoshida, K., Hirajima, T., Ohsawa, S., Kobayashi, T., Mishima, T., and Sengen, Y., 2015, Geochemical features and relative B-Li-Cl compositions of deep-origin fluids trapped in high-pressure metamorphic rocks: Lithos, v. 226, p. 50–64, doi: 10.1016/j.lithos.2015.03.002.

Yoshida, T., Kimura, J.-I., Yamada, R., Acocella, V., Sato, H., Zhao, D., Nakajima, J., Hasegawa, A., Okada, T., Honda, S., Ishikawa, M., Prima, O.D. a., Kudo, T., Shibazaki, B., et al., 2014a, Evolution of late Cenozoic magmatism and the crust-mantle structure in the NE Japan Arc: Geological Society, London, Special Publications, v. 385, no. 1, p. 335–387, doi: 10.1144/SP385.15.

Yoshida, T., Kimura, J.-I., Yamada, R., Acocella, V., Sato, H., Zhao, D., Nakajima, J., Hasegawa, A., Okada, T., Honda, S., Ishikawa, M., Prima, O.D.A., Kudo, T., Shibazaki, B., et al., 2014b, Evolution of late Cenozoic magmatism and the crust–mantle structure in the NE Japan Arc: Geological Society, London, Special Publications, v. 385, no. 1, p. 335–387, doi: 10.1144/SP385.15.

Zhao, D., Horiuchi, S., and Hasegawa, A., 1992, Seismic velocity structure of the crust beneath the Japan Islands: Tectonophysics, v. 212, no. 3–4, p. 289–301, doi: 10.1016/0040-1951(92)90296-I.